Supporting Information for:

Ultrafast non-adiabatic dynamics of excited diphenylmethyl bromide elucidated by quantum dynamics and semi-classical on- the-fly dynamics.

Specially adapted reactive coordinates

The concept of specially adapted reactive coordinates developed in our group is used to build the reduced coordinate space for the QD simulation.[1] A relaxed scan along the C_1-Br bond length at the B3LYP/6-31G(d) level of theory is used as basis to build sigmoidal fit function for important coordinates in relation to the reactive coordinate *r* (see Figure S1 for atom labeling). Important coordinates are e.g. bond length and angles associated with the central carbon atom C_1 and the relative positions of the phenyl rings. The fit functions are hereby of the form

$$f(r) = a \cdot \frac{1}{1 + e^{b \cdot (r-c)}} + d,$$

with the corresponding fit parameters listed in Table S1. For the second reactive coordinate d_{py}, the sigmoidal fit function is built symmetric for positive and negative values with a maximum distance r at $d_{py} = 0.0$ Å. The first step of building the quasi relaxed geometries is, to calculate a $r'(d_{py})$ by using the inverse of the fit function $f_{d_{py}}(r)$:

$$r'(d_{py}) = f_{d_{py}}^{-1}(r) = \frac{1}{\mathrm{b}} \cdot \log\left(\frac{a}{d_{py} - d} - 1\right) + c$$

Then all other selected coordinates are calculated with this bond length $r'(d_{py})$ so that the coordinates are given in relation to the coordinate d_{py}. As last step, the C_1-Br distance is adjusted. The angles of the Br atom to the atoms C_2, C_3 and H (Br-C_1-C_2, Br-C_1-C_3, Br-C_1-H) are kept constant at the corresponding values at the ground state minimum (B3LYP/6-31G(d)). The bond lengths and angles within the phenyl rings are kept constant, as well.

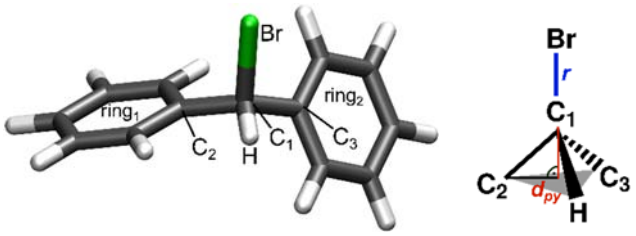

Figure S1. Ground state geometry of Ph_2CH-Br at the ONIOM(CAS(12,10):B3LYP) level of theory with atom labeling and reactive coordinates *r* and d_{py}.

Table S1. Parameters of the fitted sigmoidal functions for the specially adapted reactive coordinates.

	a	b	c	d
d_{py}	0.6537	2.3476	2.2070	0.0
C_2-C_1	0.1540	2.27361	2.0231	1.4374
C_1-C_3	0.1563	2.2141	2.1645	1.4176
C_2-C_1-C_3	-24.0039	2.6579	1.9611	128.4262
C_2-C_1-H	-18.1708	2.9148	1.9045	116.8425
$ring_1$/C_1-C_3	45.6242	2.3425	2.6571	1.7711
$ring_1$/$ring_2$	92.2834	2.0590	1.7711	38.3191

Computational details of the quantum dynamical simulation

We used a simulation grid with 1536×2048 $(r \times d_{py})$ grid points from $r = 1.5 - 20$ Å and $d_{py} = -0.6 - 0.7$ Å. For the simulation, the first vibrational eigenfunction of the electronic ground state is obtained by propagating in imaginary time.[2] A dipole-laser excitation from the ground state to the $\pi\pi^*$ state with a gaussian laser pulse $\left(FWHM = 18 \text{ fs}; \lambda = 250 \text{ nm}; I_{max} = 5.63 \cdot 10^{13} \frac{\text{W}}{\text{cm}^2};\ t_0 = 0 \text{ fs}\right)$ is employed. The Chebychev propagator[3] is used with a time step of $\Delta t = 10$ au. To avoid unphysical effects occurring when the wave packet reaches the border of the simulation grid a gobbler operator is used to cut off the wave packet from a certain value at the border of the grid.

The potential energy surface are shown in Figure S2 in single contour representation. The G-Matrix elements[1, 4-6] describing the kinetic energy operator in the reduced coordinate space can be seen in Figure S3. The diabatic coupling matrix elements (DCMEs) were calculated using the transition dipole moment as described in reference 7 (Figure S4). Figure S5 shows the first vibrational eigenfunction of the ground state and the slightly shifted wave packet. The wave packet in the $\pi\pi^*$ minimum after laser excitation is shown in Figure S6.

Integral of the wave packet

The discrete integral of the wave packet as a function of time is calculated as

$$F(t) = \frac{\sum_{k=y_{min}}^{y_{max}} \sum_{l=x_{min}}^{x_{max}} \Psi^s\left(d_{py_k}, r_l, t\right)^* \Psi^s\left(d_{py_k}, r_l, t\right) \Delta r \Delta d_{py}}{\sum_{k}^{N_{dpy}} \sum_{l=1}^{N_r} \Psi^s\left(d_{py_k}, r_l, t_{ref}\right)^* \Psi^s\left(d_{py_k}, r_l, t_{ref}\right) \Delta r \Delta d_{py}},$$

where N_r is the number of grid points in the coordinate r and N_{dpy} the number of grid points in the coordinate d_{py} and Δr and Δd_{py} the grid spacing. x_{min}, x_{max}, y_{min} and y_{max} are the integration barriers of the wave packet, $\Psi^s\left(d_{py_k}, r_l, t\right)$ is the wave packet at point t of state s and $\Psi^s\left(d_{py_k}, r_l, t_{ref}\right)$ is the reference wave packet at the point in time of maximal population in state s. The restricted area for the integration is set to $x_{min} = 1.5$ Å, $x_{max} = 20.0$ Å, $y_{min} = -0.005$ Å, $y_{max} = 0.005$ Å in the $n_1\pi^*$ state and along the $CoIn_1$ seam in the $\pi\pi^*$ state from $x_{min} = 2.3$ Å, $y_{min} = -0.118$ Å to $x_{max} = 2.4$ Å, $y_{max} = 0.412$ Å.

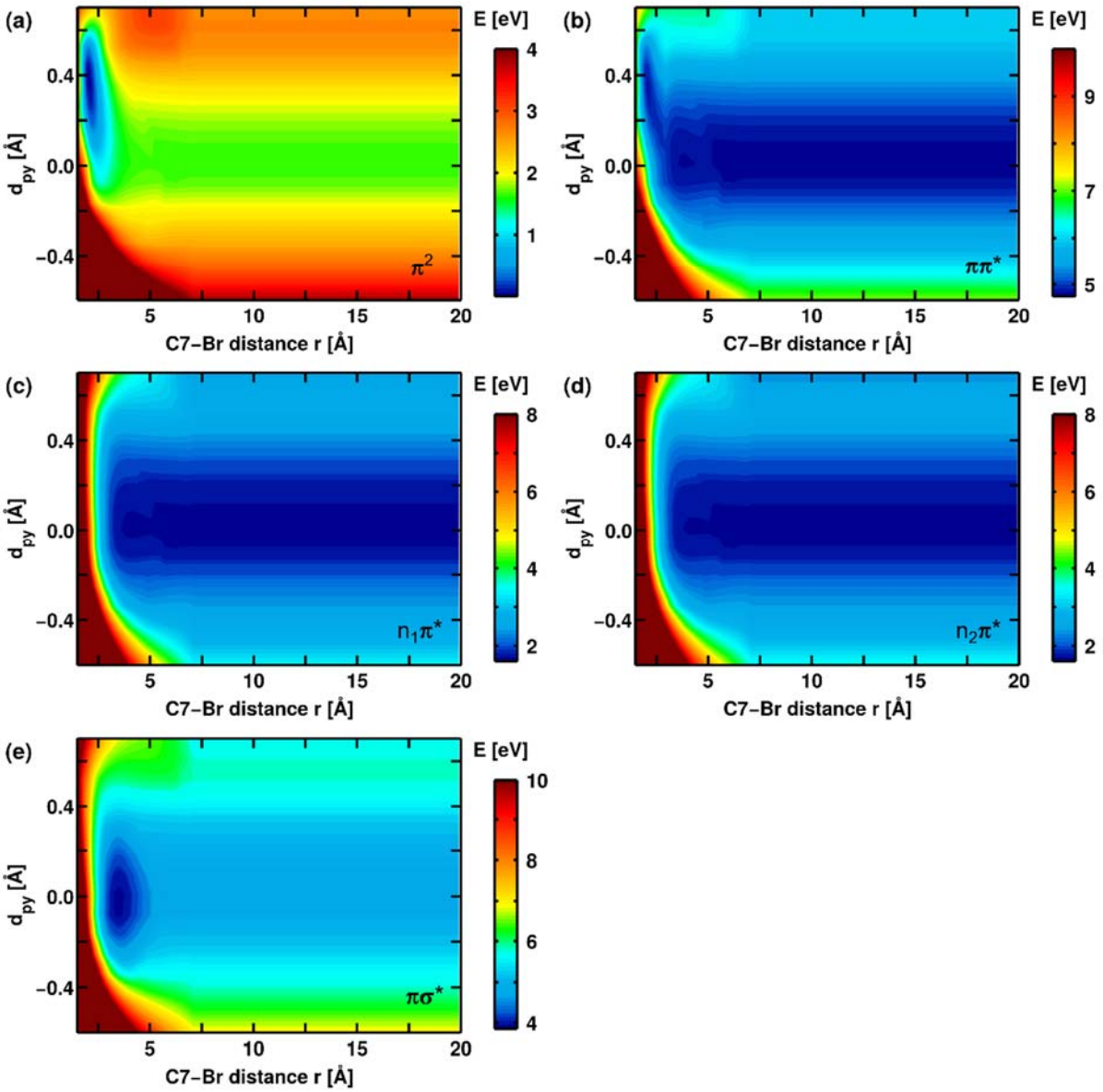

Figure S2. Diabatic potential energy surfaces of the five lowest singlet states at the ONIOM(CASSCF:B3LYP)/6-31G(d) level of theory along the distances r and d_{py}. a) Ground state (π^2) with minimum at $r = 1.8$ Å and $d_{py} = 0.4$ Å. b) $\pi\pi^*$ state with a minimum in the Franck-Condon region. c) and d) the degenerated $n_1\pi^*$ and $n_2\pi^*$ states describing the homolytic bond cleavage channel. e) $\pi\sigma^*$ state describing the heterolytic bond cleavage channel with a minimum shifted in negative d_{py} direction from the Franck-Condon region.

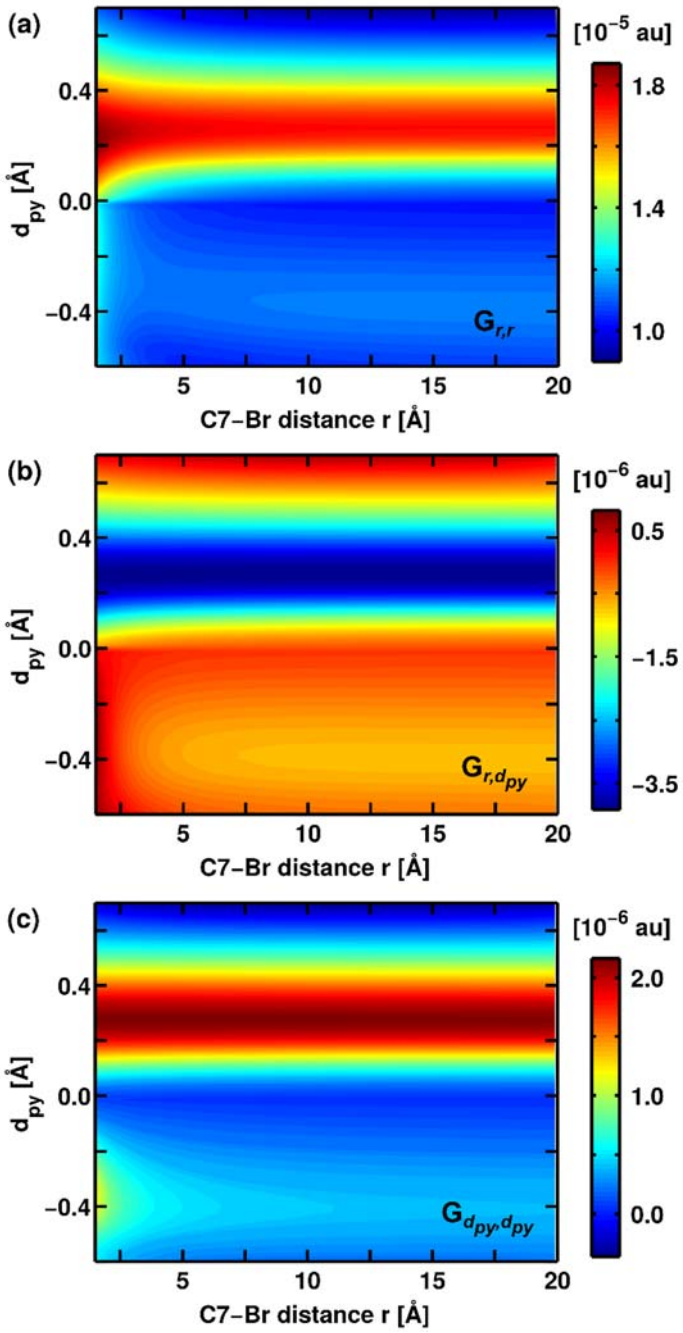

Figure S3. G-Matrix elements along the coordinates r and d_{py}. a) Diagonal element $\boldsymbol{G_{rr}}$, b) off-diagonal element $\boldsymbol{G_{rd_{py}}}$ and c) second diagonal element $\boldsymbol{G_{d_{py}d_{py}}}$. The element $\boldsymbol{G_{rr}}$ is one magnitude larger than the other two elements. The largest changes occur within the coordinate d_{py} while the elements do not change significantly with the coordinate r. The G-Matrix elements are of the form $G_{ab} = \sum_{i=1}^{3N} \frac{1}{m_i} \frac{\partial q_a}{\partial x_i} \frac{\partial q_b}{\partial x_i}$. They are calculated via its inverse $(G^{-1})_{ab}$ using the finite difference method.[8] q_a, q_b are the internal coordinates and x_i the Cartesian coordinates with the corresponding atomic masses m_i and the number of atoms N.

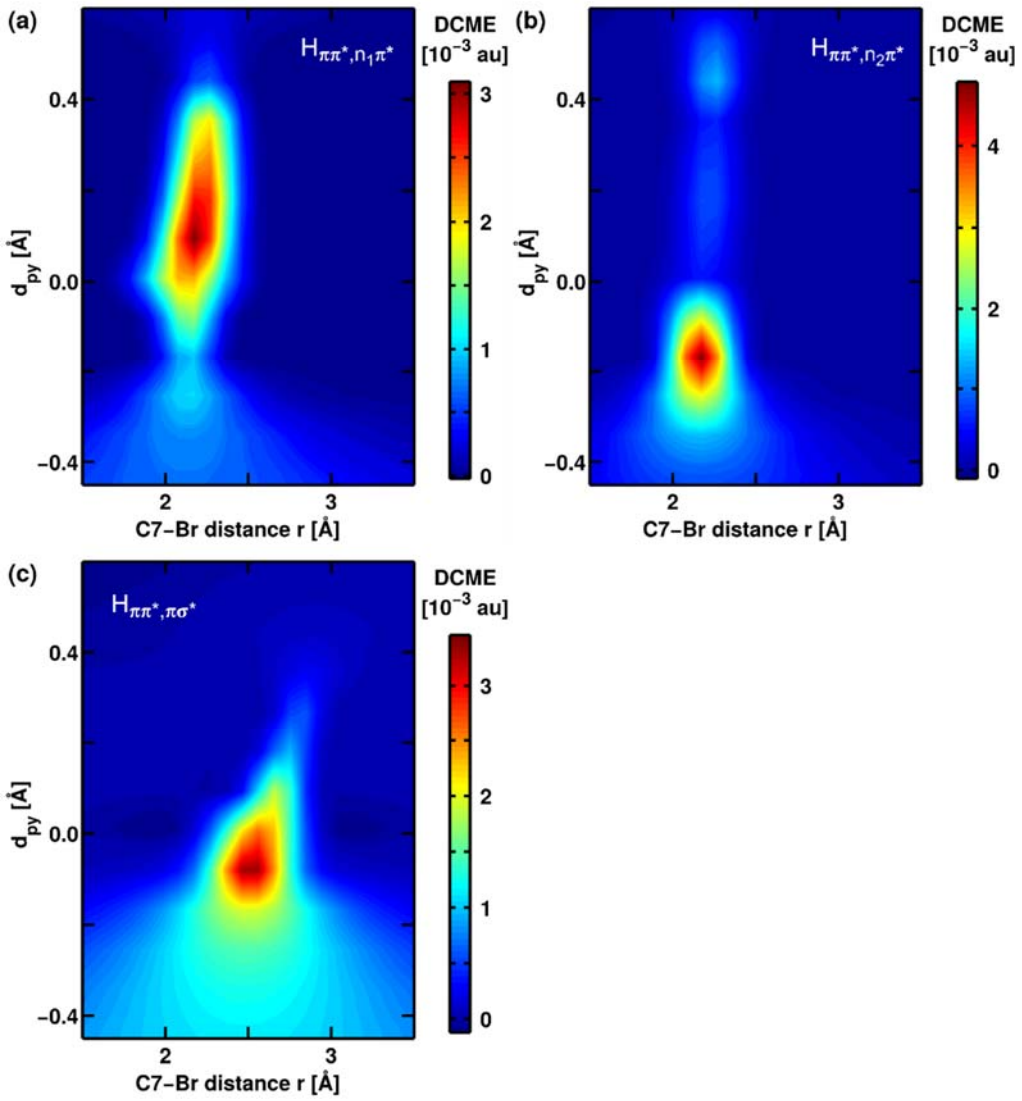

Figure S4. Diabatic coupling matrix elements between the $\pi\pi^*$ state and a) the $n_1\pi^*$, b) the $n_2\pi^*$ and c) the $\pi\sigma^*$ state. The coupling elements of the two degenerated lone pair states are different because of the orthogonal position of the lone pair orbitals of the bromine atom. In the area of positive d_{py} values, the first lone pair orbital has a better position to the π orbitals of the one phenyl ring included in the active space. With negative d_{py} values the situation changes and the second element has a larger coupling element. This makes the $n_1\pi^*$ state more important than the $n_2\pi^*$ state because the coupling in the FC region is larger in the first case. This can be seen when evaluating the population of the two $n\pi^*$ states separately. The first accounts hereby for more than 90 % while the second only accounts for less than 10 %. This matter vanishes when orbitals of both phenyl rings are included in the active space because then each lone pair orbital has a better position to one of the phenyl rings making them completely equal again. The maximum of the third coupling element (c) is also shifted from the FC region and therefore the $\pi\sigma^*$ state is also less important.

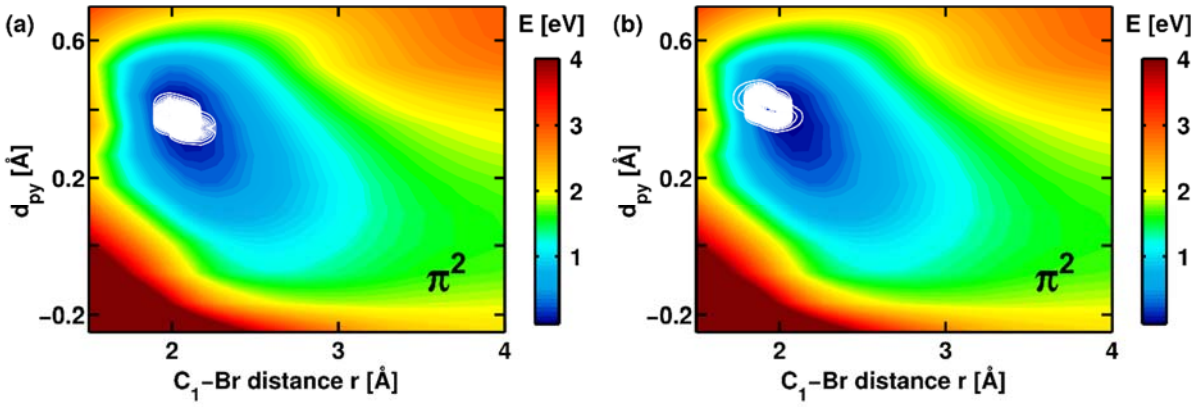

Figure S5. Ground state minimum with a) the first vibrational eigenfunction and b) the shifted wave packet.

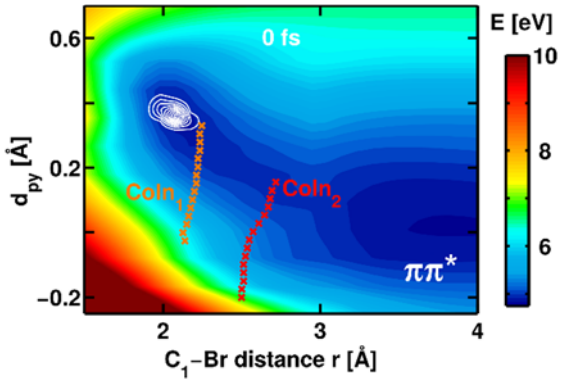

Figure S6. Wave packet in the $\pi\pi^*$ minimum after laser excitation at $t = 0$ fs. The seam of $CoIn_1$ is shown in orange and the seam of $CoIn_2$ in red.

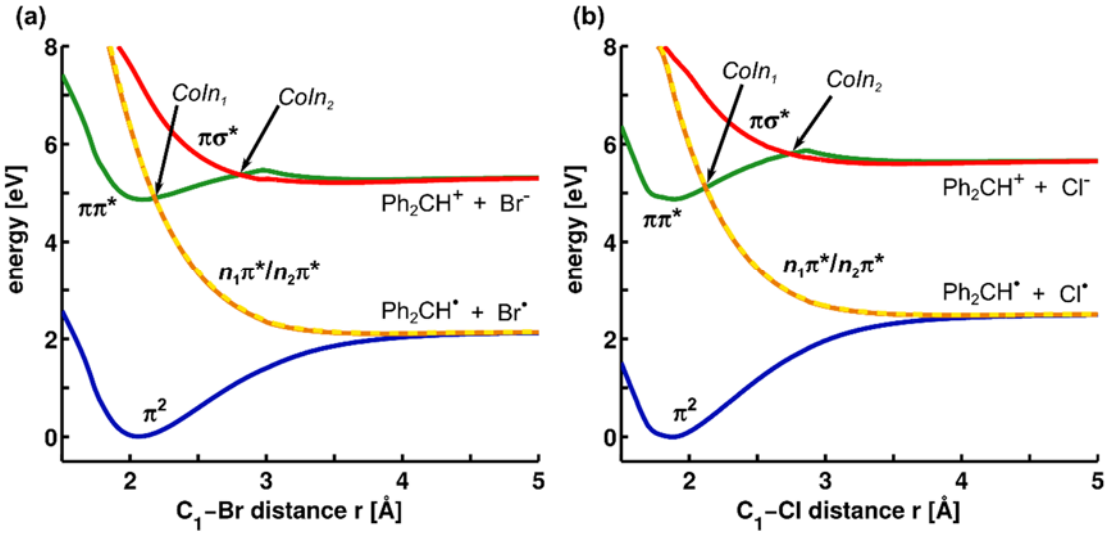

Figure S7. One dimensional diabatic PES of a) Ph_2CHBr at constant $d_{py} = 0.35\,\text{Å}$ and b) Ph_2CHCl at constant $d_{py} = 0.4$ Å along the C_1-X bond. The main differences are the location of the FC point in the coordinate r and the relative positions of the CoIns to the respective S_1 minimum. The barriers are higher in the case of Ph_2CHCl compared to Ph_2CHBr.

Spectrogram from the velocity autocorrelation function

The spectrograms[9, 10] are calculated using the velocity autocorrelation function $C_v(t)$

$$C_v(t) = \frac{1}{N}\sum_{j=1}^{N} v_j(0) \cdot v_j(t),$$

with the dot product $v_j(0) \cdot v_j(t)$ of the velocity of atom j at time 0 and time t and the number of atoms N. The time resolution is obtained using a Short-time Fourier transform[9] for a joint time-frequency representation:

$$S(\tau, \omega) = \frac{1}{n}\sum_{k=1}^{n}\left|\frac{1}{2\pi}\int_0^{\infty} C_v^k(t) \cdot G(t,\tau) \cdot e^{-i\omega t} dt\right|^2,$$

with the number of trajectories *n*, the frequency ω and the Gaussian window function

$$G(t,\tau) = \frac{1}{\sqrt{2\pi}\sigma}\exp\left(-\frac{1}{2}\left(\frac{t-\tau}{\sigma}\right)^2\right),$$

with the window pulse width $\sigma = 125$ fs. Please note that the short-time spectrogram of homolytic bond cleavage is only averaged over 23 trajectories (Figure S8a) and the spectrogram of heterolytic bond cleavage over 21 trajectories (Figure S8b). The long-time spectrograms (Figure S9) are averaged over the respective total sum of trajectories.

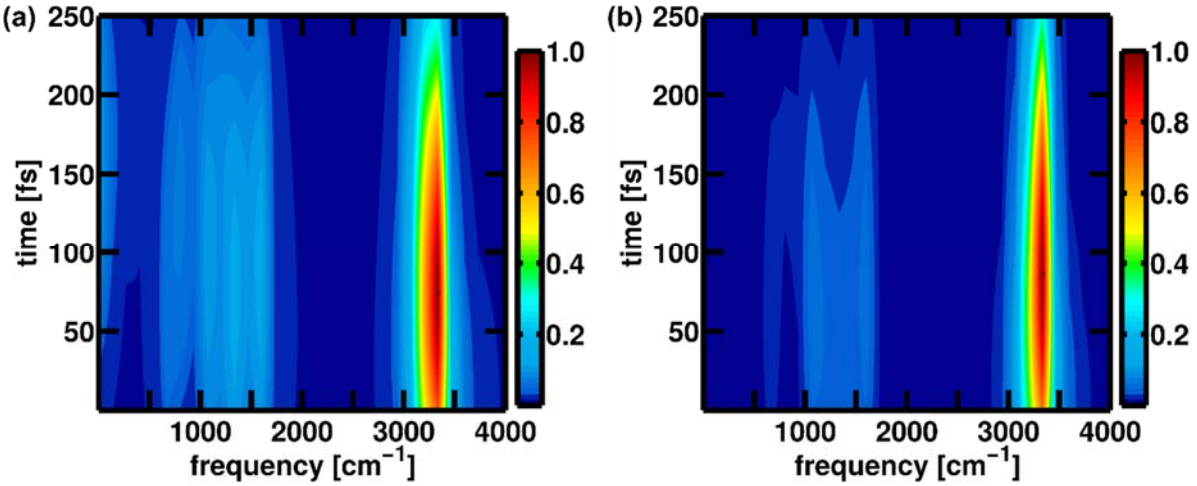

Figure S8. Spectrogram of a) the trajectories of homolytic bond cleavage and b) the trajectories of heterolytic bond cleavage. The strongest band of both spectra lies at $\nu = 3300$ cm^{-1} which can be assigned to C-H stretch motions activated by the Wigner distribution.

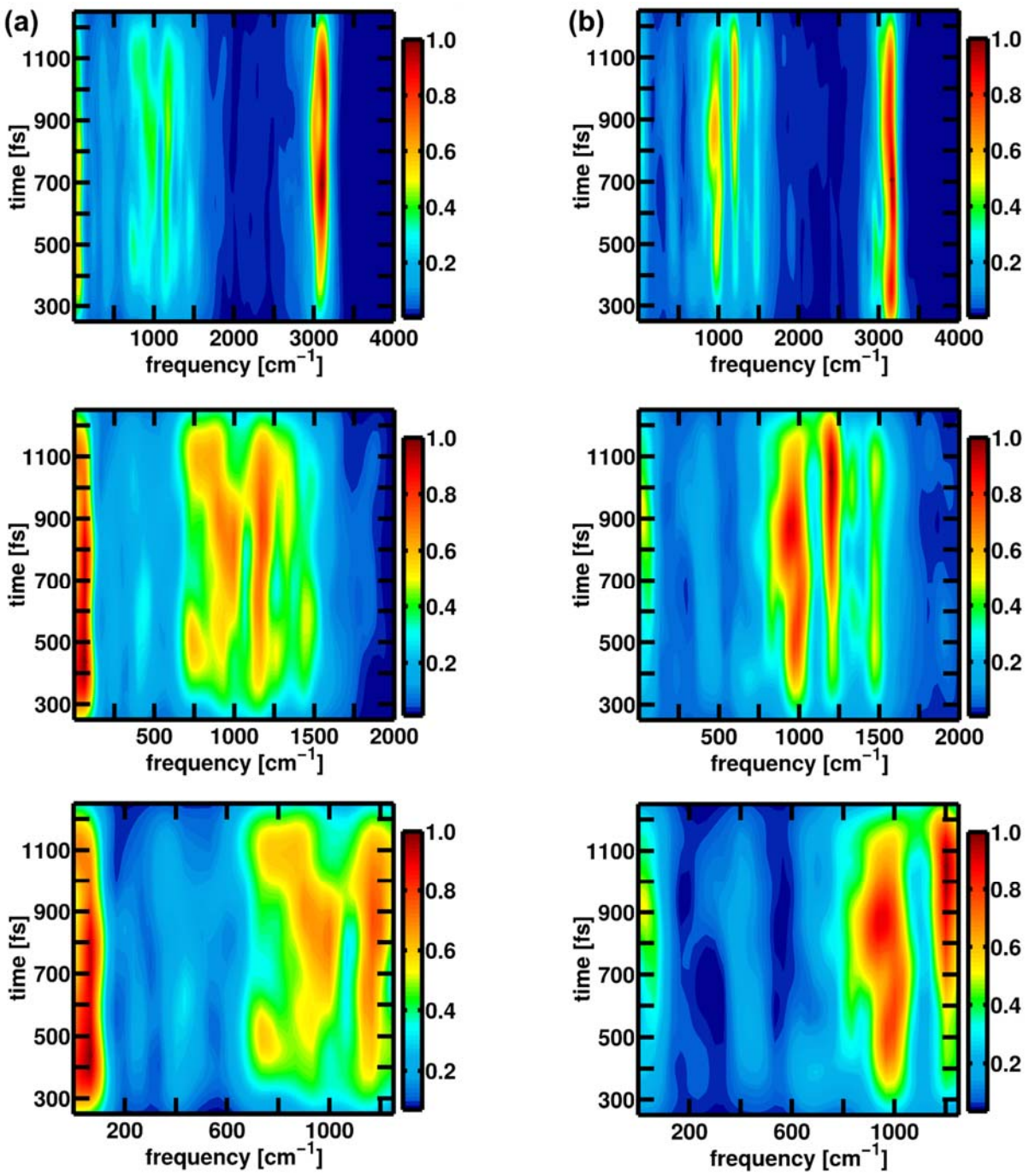

Figure S9. Spectrogram of a) the $Ph_2CH^{\bullet}$ trajectories and b) the Ph_2CH^{+} trajectories with different frequency areas.

Active Space (12,10)

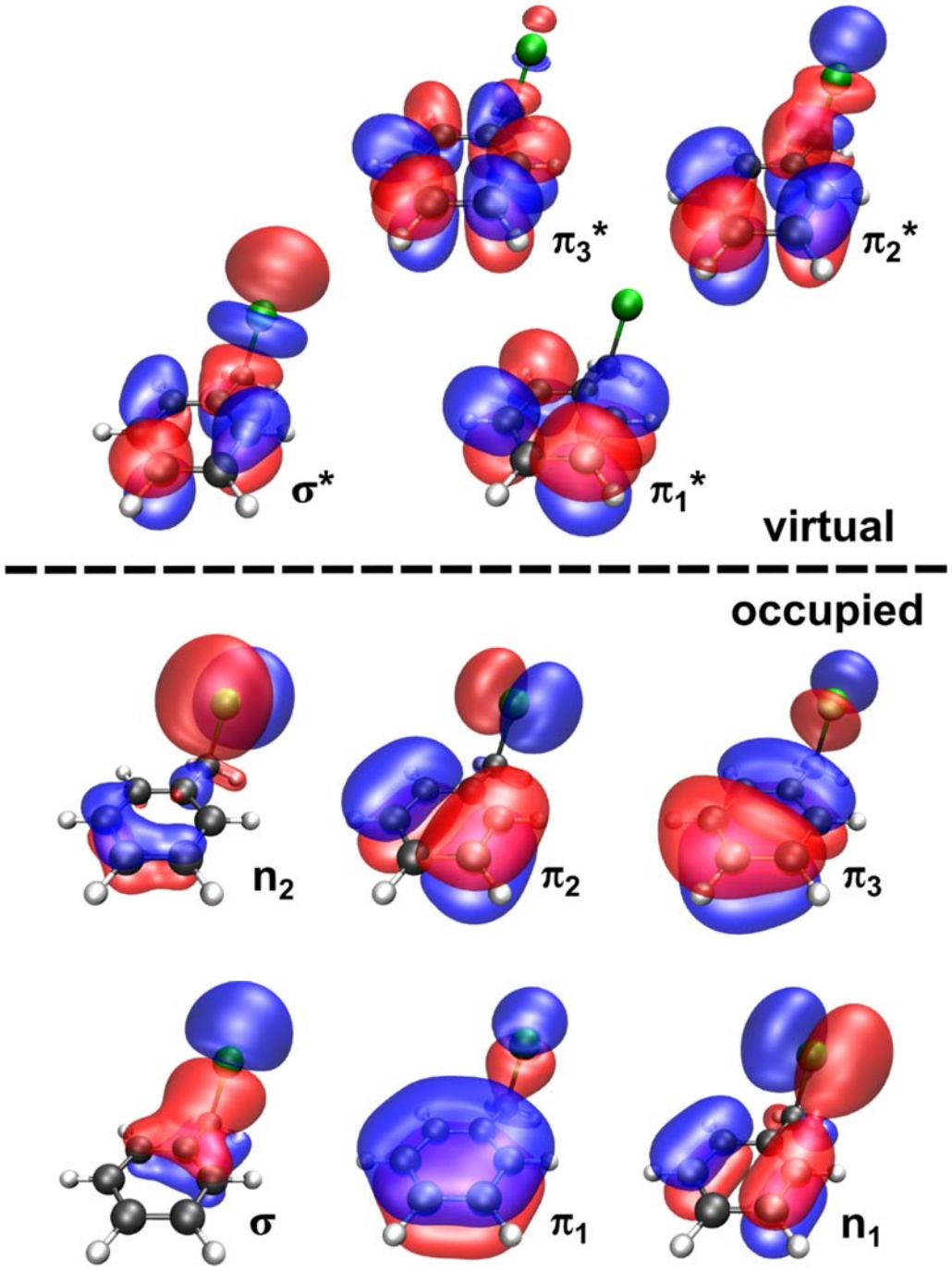

Figure S10. Active space of the CAS(12,10) calculations. It includes the complete π orbital space of one phenyl ring, the two lonepair orbitals of the bromine atom (n_1, n_2) and the σ/σ^* orbitals of the C_1-Br bond.

Normal mode vectors of Ph_2CH-Br

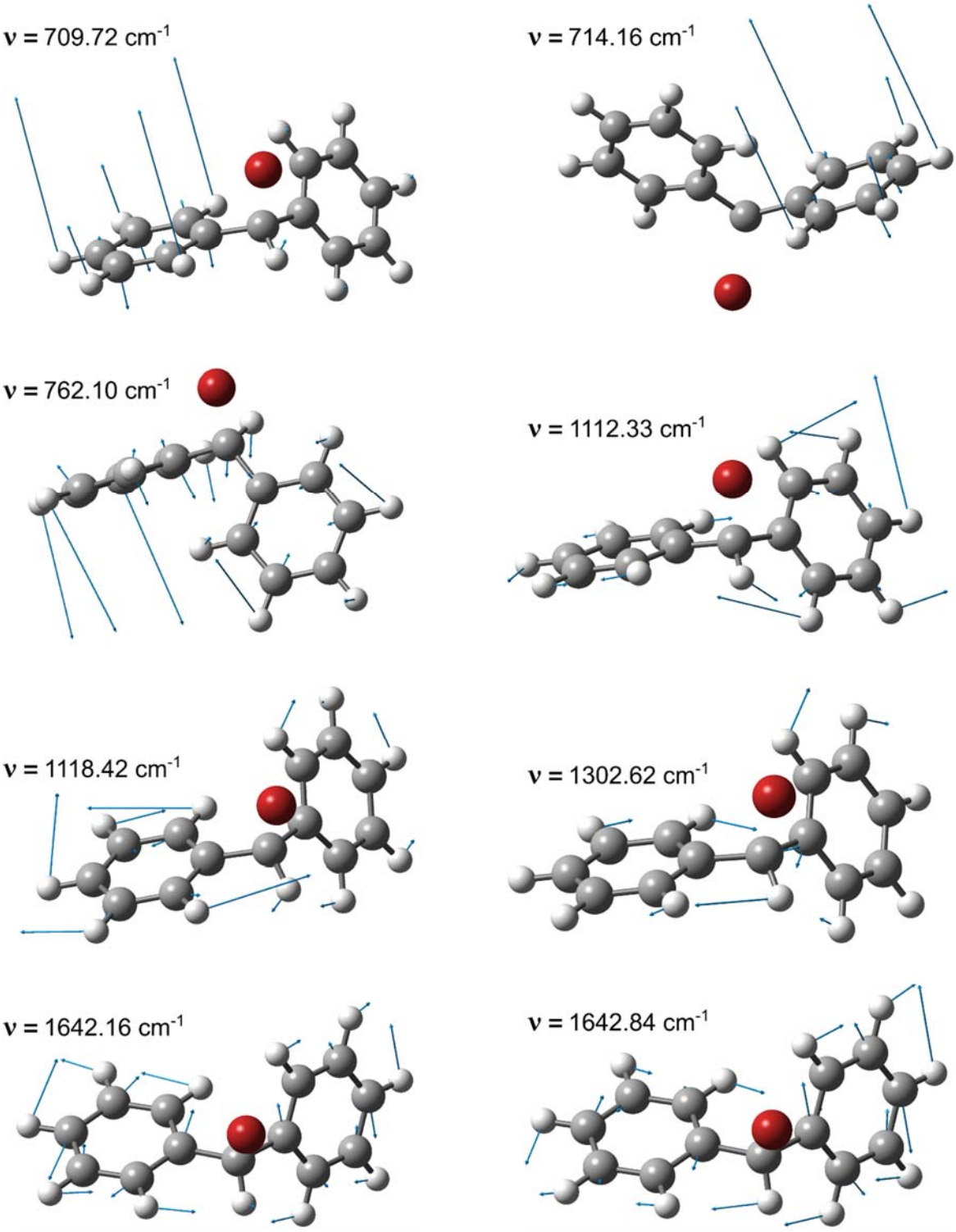

Figure S11. Normal mode vectors of Ph_2CH-Br of the frequency analysis at the ground state minimum at B3LYP level of theory.

Normal mode vectors of $Ph_2CH^{\bullet}$ and Ph_2CH^{+}

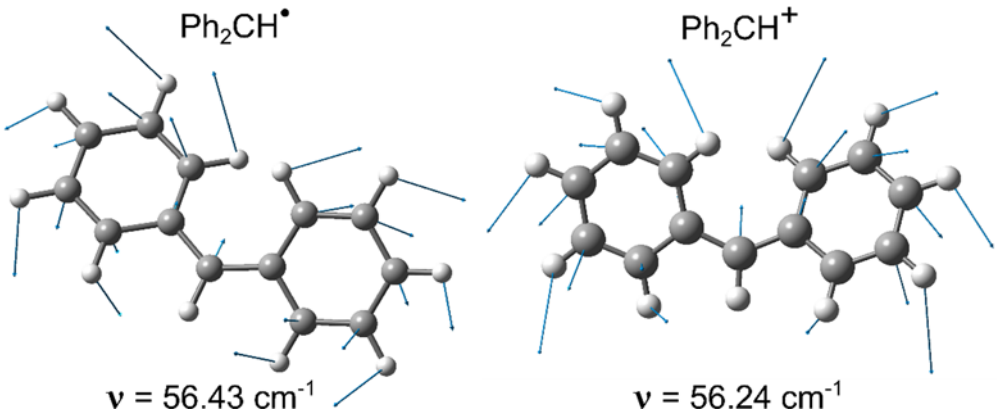

Figure S12. Normal mode vectors of $Ph_2CH^{\bullet}$ and Ph_2CH^{+} at the respective ground state at B3LYP level of theory.

Spin-orbit coupling of $PhCH_2Br$ along the dissociation pathway

Relevant spin-orbit coupling (SOC) elements of the model system $PhCH_2Br$ at the CASSCF(12,10) level of theory. Five singlet and five triplet states were included in the calculations. For the S_0 minimum the S_1 ππ* state is chosen as state of reference for the energy difference and the SOC. For $CoIn_1$ also S_1 is chosen, additionally also the SOC of S_2 and S_3 to the triplet states are shown as all three singlet states are close together. At $CoIn_2$ the adiabatic S_3 is state of reference, which is now the ππ* state. For the grid point at large r the energy difference to S_0 is specified, the SOC between all singlet and triplet states is given.

S_0 minimum

	abs. energy [Hartree]	ΔE(X,S1) [eV]	SOC(Tn,S1) [cm^{-1}]
S0	-2838.83558	-4.82	/
S1	-2838.65843	0.00	/
S2	-2838.60566	1.44	/
S3	-2838.60498	1.45	/
S4	-2838.55809	2.73	/
T1	-2838.70003	-1.13	18.04
T2	-2838.65726	0.03	2.85
T3	-2838.65662	0.05	0.60
T4	-2838.62634	0.87	4.56
T5	-2838.62595	0.88	22.65

$CoIn_1$

	abs. energy [Hartree]	ΔE(X,S1) [eV]	SOC(Tn,S1) [cm^{-1}]	SOC(Tn,S2) [cm^{-1}]	SOC(Tn,S3) [cm^{-1}]
S0	-2838.81809	-4.59	/	/	/
S1	-2838.6493	0.00	/	/	/
S2	-2838.64358	0.16	/	/	/
S3	-2838.64345	0.16	/	/	/
S4	-2838.56972	2.17	/	/	/
T1	-2838.69183	-1.16	24.01	269.14	175.28
T2	-2838.65741	-0.22	17.80	557.95	91.47
T3	-2838.65731	-0.22	32.27	106.60	573.43
T4	-2838.64838	0.03	6.72	367.20	229.85
T5	-2838.64606	0.09	6.95	168.32	125.66

$CoIn_2$

	abs. energy [Hartree]	ΔE(X,S3) [eV]	SOC(Tn,S3) [cm^{-1}]	SOC(Tn,S4) [cm^{-1}]
S0	-2838.77947	-3.34	/	/
S1	-2838.73246	-2.06	/	/
S2	-2838.73092	-2.02	/	/
S3	-2838.65679	0.00	/	/
S4	-2838.65089	0.16	/	/
T1	-2838.74443	-2.38	10.80	226.50
T2	-2838.73298	-2.07	7.26	331.89
T3	-2838.73274	-2.07	5.43	283.46
T4	-2838.65739	-0.02	1.67	102.99
T5	-2838.64595	0.29	32.69	155.09

Grid point of QD simulation: $d_{py} = 0.05$ Å , $r = 4.0$ Å

	abs. energy [Hartree]	ΔE(X,S0) [eV]	SOC(Tn,S0) [cm^{-1}]	SOC(Tn,S1) [cm^{-1}]	SOC(Tn,S2) [cm^{-1}]	SOC(Tn,S3) [cm^{-1}]	SOC(Tn,S4) [cm^{-1}]
S0	-2838.7499	0.00	/	/	/	/	/
S1	-2838.74772	0.06	/	/	/	/	/
S2	-2838.74707	0.08	/	/	/	/	/
S3	-2838.64698	2.80	/	/	/	/	/
S4	-2838.63256	3.19	/	/	/	/	/
T1	-2838.74863	0.03	312.46	807.14	797.56	43.86	3.67
T2	-2838.74759	0.06	820.25	326.81	525.36	60.17	4.34
T3	-2838.74716	0.07	760.61	551.92	23.77	56.87	3.86
T4	-2838.63308	3.18	1.58	3.83	4.21	50.03	111.03
T5	-2838.63160	3.22	1.54	0.46	1.43	76.94	877.92

Coordinates of optimized geometries

The optimizations of the model system phenylmethyl bromide at the CASSCF level of theory were performed with the program package MOLPRO2012[11, 12]. Only the optimization of the three-state conical intersection $CoIn_1$ was performed with the program Columbus[13-15]. The S_0 minimum of the complete system diphenylmethyl bromide was calculated at B3LYP level of theory with the program package Gaussian09[16] and at ONIOM(CASSCF:HF) level of theory with the program package MOLPRO2012 and a code of our own design for the ONIOM part. For all calculations we employed the binning-SVP basis set for the bromine atom and the 6-31G(d) basis set for all other atoms.

PhCH$_2$−Br: S_0 minimum, CAS(12,10)			
Absolute energy: -2838.835256 Hartree			
C	-2.418824	-0.140437	0.992942
C	-1.263260	-0.339854	0.224015
C	-1.256714	-1.358337	-0.739175
C	-2.378727	-2.166988	-0.923940
C	-3.524738	-1.964570	-0.149742
C	-3.541633	-0.947211	0.809108
C	-0.059943	0.521128	0.428859
Br	-0.106382	2.192756	-0.701275
H	0.021659	0.893713	1.435226
H	-0.379719	-1.516266	-1.342007
H	-2.358546	-2.947479	-1.662887
H	-4.388933	-2.587921	-0.291086
H	-4.419721	-0.785263	1.407714
H	-2.440711	0.645591	1.727219
H	0.856857	0.036282	0.140461

PhCH$_2$−Br: S_1 minimum, CAS(12,10)			
Absolute energy: -2838.665381 Hartree			
C	-2.405402	-0.142668	1.048136
C	-1.197148	-0.369565	0.292697
C	-1.215704	-1.384352	-0.732983
C	-2.386146	-2.186582	-0.951638
C	-3.565743	-1.973163	-0.171527
C	-3.573796	-0.946609	0.824201
C	-0.039455	0.520693	0.445604
Br	-0.177690	2.175274	-0.775896
H	0.047204	0.956848	1.425539
H	-0.342393	-1.541461	-1.337487
H	-2.370080	-2.947404	-1.708111
H	-4.440309	-2.571289	-0.338789
H	-4.455593	-0.769678	1.409423
H	-2.429726	0.637687	1.785160
H	0.892644	0.077415	0.141100

PhCH$_2$–Br: $CoIn_1$, CAS(12,10)			
Absolute energy: -2838.644059 Hartree			
C	0.381431	-0.372186	-2.705196
C	0.384960	-0.251096	-1.293822
C	1.644296	-0.223414	-0.593400
C	2.858198	-0.436317	-1.257719
C	2.823029	-0.594618	-2.679695
C	1.614082	-0.544305	-3.385184
C	-0.827339	-0.282315	-0.442899
Br	-2.257192	1.253675	-1.141292
H	-1.408565	-1.168740	-0.428055
H	1.628068	-0.113877	0.474519
H	3.770606	-0.531869	-0.704793
H	3.732574	-0.743875	-3.224804
H	1.624163	-0.658747	-4.455556
H	-0.550486	-0.269572	-3.265430
H	-0.725503	0.174048	0.555877

PhCH$_2$–Br: $CoIn_2$, CAS(12,10)			
Absolute energy: -2838.656343 Hartree			
C	0.430369	-0.416639	-2.702893
C	0.382321	-0.472034	-1.250915
C	1.668987	-0.464476	-0.572398
C	2.899239	-0.407933	-1.308479
C	2.901354	-0.357962	-2.712568
C	1.678973	-0.360260	-3.406721
C	-0.804332	-0.500999	-0.563240
Br	-1.088585	2.276295	-0.353002
H	-1.741260	-0.576033	-1.080003
H	1.691214	-0.485554	0.499966
H	3.825540	-0.401849	-0.765999
H	3.828775	-0.314137	-3.250864
H	1.665826	-0.317519	-4.479226
H	-0.490762	-0.399832	-3.252661
H	-0.822769	-0.609388	0.503765

Ph_2CH-Br: S_0 minimum, B3LYP			
Absolute energy: -3073.719707 Hartree			
C	-2.494458	-0.017452	0.794170
C	-1.246102	-0.402910	0.277824
C	-1.175093	-1.550507	-0.519712
C	-2.326500	-2.290003	-0.802500
C	-3.560530	-1.896329	-0.289043
C	-3.640457	-0.754246	0.514021
C	-0.025950	0.409956	0.647279
Br	-0.190804	2.245941	-0.222937
H	-0.073526	0.677638	1.703050
H	-0.218770	-1.876851	-0.913376
H	-2.252026	-3.178465	-1.423869
H	-4.454752	-2.473286	-0.508833
H	-4.597388	-0.439222	0.921406
H	-2.562969	0.881729	1.401334
C	1.325454	-0.179434	0.334716
C	1.841232	-0.228895	-0.968098
C	3.072149	-0.832133	-1.218323
C	3.808620	-1.391858	-0.170772
C	3.307105	-1.340375	1.129487
C	2.074131	-0.735099	1.379555
H	1.282913	0.232453	-1.777074
H	3.461445	-0.858119	-2.232547
H	4.770844	-1.856831	-0.367405
H	3.875934	-1.764343	1.952571
H	1.688838	-0.696946	2.395915

Ph_2CH-Br: S_0 minimum, ONIOM(CASSCF:HF) Absolute energy: -3068.375786 Hartree			
C	-2.379011	-0.151924	0.979439
C	-1.232735	-0.364772	0.198002
C	-1.254445	-1.384423	-0.763789
C	-2.395303	-2.169785	-0.937542
C	-3.531180	-1.951554	-0.153492
C	-3.518401	-0.937502	0.808300
C	-0.029633	0.515963	0.423099
Br	-0.219650	2.206033	-0.698967
H	-0.074253	0.927828	1.416680
H	-0.387213	-1.575348	-1.366317
H	-2.394019	-2.949948	-1.677273
H	-4.406783	-2.560555	-0.287169
H	-4.385136	-0.761251	1.419429
H	-2.382530	0.633336	1.715076
C	1.325220	-0.128490	0.221203
C	1.973310	-0.200920	-1.005530
C	3.188050	-0.856560	-1.119524
C	3.774003	-1.445646	-0.010893
C	3.137265	-1.373529	1.216448
C	1.922536	-0.717710	1.329803
H	1.539813	0.269135	-1.867424
H	3.678806	-0.899758	-2.075166
H	4.719453	-1.949271	-0.101790
H	3.584652	-1.820932	2.085657
H	1.436523	-0.668004	2.288581

References

1. S. Thallmair, M. K. Roos and R. de Vivie-Riedle, *J. Chem. Phys.*, 2016, 144, 234104.
2. R. Kosloff and H. Tal-Ezer, *Chemical Physics Letters*, 1986, 127, 223-230.
3. H. Tal-Ezer and R. Kosloff, *J. Chem. Phys.*, 1984, 81, 3967.
4. B. Podolsky, *Phys. Rev.*, 1928, 32, 812-816.
5. E. B. Wilson, J. C. Decius and P. C. Cross, *Molecular Vibrations: The Theory of Infrared and Raman Vibrational Spectra*, Dover Publ., New York, 1980.
6. L. J. Schaad and J. Hu, *J. Mol. Struct.: THEOCHEM*, 1989, 185, 203-215.
7. S. Thallmair, M. K. Roos and R. de Vivie-Riedle, *Struct. Dyn.*, 2016, 3, 043205.
8. V. Alexandrov, D. M. A. Smith, H. Rostkowska, M. J. Nowak, L. Adamowicz and W. McCarthy, *J. Chem. Phys.*, 1998, 108, 9685.
9. M. Tamaoki, Y. Yamauchi and H. Nakai, *J. Comput. Chem.*, 2005, 26, 436-442.
10. B. P. Fingerhut, PhD Thesis, Ludwigs-Maximilians-Universität, 2010.
11. H. J. Werner, P. J. Knowles, G. Knizia, F. R. Manby, M. Schütz, P. Celani, T. Korona, R. Lindh, A. Mitrushenkov, G. Rauhut, K. R. Shamasundar, T. B. Adler, R. D. Amos, A. Bernhardsson, A. Berning, D. L. Cooper, M. J. O. Deegan, A. J. Dobbyn, F. Eckert, E. Goll, C. Hampel, A. Hesselmann, G. Hetzer, T. Hrenar, G. Jansen, C. Köppl, Y. Liu, A. W. Lloyd, R. A. Mata, A. J. May, S. J. McNicholas, W. Meyer, M. E. Mura, A. Nicklass, D. P. O'Neill, P. Palmieri, D. Peng, K. Pflüger, R. Pitzer, M. Reiher, T. Shiozaki, H. Stoll, A. J. Stone, R. Tarroni, T. Thorsteinsson and M. Wang, MOLPRO, version 2012.1, a package of *ab initio* programs, 2012, see www.molpro.net.
12. H.-J. Werner, P. J. Knowles, G. Knizia, F. R. Manby and M. Schütz, *WIREs Comput. Mol. Sci.*, 2012, 2, 242-253.
13. H. Lischka, R. Shepard, I. Shavitt, R. M. Pitzer, M. Dallos, T. Müller, P. G. Szalay, F. B. Brown, R. Ahlrichs, H. J. Böhm, A. Chang, D. C. Comeau, R. Gdanitz, H. Dachsel, C. Ehrhardt, M. Ernzerhof, P. Höchtl, S. Irle, G. Kedziora, T. Kovar, V. Parasuk, M. J. M. Pepper, P. Scharf, H. Schiffer, M. Schindler, M. Schüler, M. Seth, E. A. Stahlberg, J.-G. Zhao, S. Yabushita, Z. Zhang, M. Barbatti, S. Matsika, M. Schuurmann, D. R. Yarkony, S. R. Brozell, E. V. Beck, J.-P. Blaudeau, M. Ruckenbauer, B. Sellner, F. Plasser and J. J. Szymczak, COLUMBUS, an *ab initio* electronic structure program, release 7.0 (2015).
14. H. Lischka, T. Müller, P. G. Szalay, I. Shavitt, R. M. Pitzer and R. Shepard, *WIREs Comput. Mol. Sci.*, 2011, 1, 191-199.
15. H. Lischka, R. Shepard, R. M. Pitzer, I. Shavitt, M. Dallos, T. Müller, P. G. Szalay, M. Seth, G. S. Kedziora, S. Yabushita and Z. Zhang, *Phys. Chem. Chem. Phys.*, 2001, 3, 664-673.
16. M. J. Frisch, G. W. Trucks, H. B. Schlegel, G. E. Scuseria, M. A. Robb, J. R. Cheeseman, G. Scalmani, V. Barone, B. Mennucci, G. A. Petersson, H. Nakatsuji, M. Caricato, X. Li, H. P. Hratchian, A. F. Izmaylov, J. Bloino, G. Zheng, J. L. Sonnenberg, M. Hada, M. Ehara, K. Toyota, R. Fukuda, J. Hasegawa, M. Ishida, T. Nakajima, Y. Honda, O. Kitao, H. Nakai, T. Vreven, J. J. A. Montgomery, J. E. Peralta, F. Ogliaro, M. Bearpark, J. J. Heyd, E. Brothers, K. N. Kudin, V. N. Staroverov, R. Kobayashi, J. Normand, K. Raghavachari, A. Rendell, J. C. Burant, S. S. Iyengar, J. Tomasi, M. Cossi, N. Rega, J. M. Millam, M. Klene, J. E. Knox, J. B. Cross, V. Bakken, C. Adamo, J. Jaramillo, R. Gomperts, R. E. Stratmann, O. Yazyev, A. J. Austin, R. Cammi, C. Pomelli, J. W. Ochterski, R. L. Martin, K. Morokuma, V. G. Zakrzewski, G. A. Voth, P. Salvador, J. J. Dannenberg, S. Dapprich, A. D. Daniels, Ö. Farkas, J. B. Foresman, J. V. Ortiz, J. Cioslowski and D. J. Fox, Gaussian 09, Revision D.01, Gaussian, Inc., Wallingford CT, 2009.